

Transit Timing Variations of the Sub-Saturn Exoplanet HAT-P-12b

Kaviya Parthasarathy^a, Hsin-Min Liu^a, Ing-Guey Jiang^{a,b}, Li-Chin Yeh^c, Napaporn A-thano^d, Supachai Awiphan^d, Wen-Chi Cheng^a, Devesh P. Sariya^a, Shraddha Biswas^e, Devendra Bisht^e, Evgeny Griv^f, David Mkrtichian^d, Vineet Kumar Mannaday^g, Prijat Thakur^h, Aleksey Shlyapnikovⁱ

^a*Institute of Astronomy, National Tsing Hua University, Hsin-Chu, Taiwan*

^b*Department of Physics, National Tsing Hua University, Hsin-Chu, Taiwan*

^c*Institute of Computational and Modeling Science, National Tsing Hua University, Hsin-Chu, Taiwan*

^d*National Astronomical Research Institute of Thailand, Chiang Mai, 50180, Thailand*

^e*Indian Centre for Space Physics, 466 Barakhola, Singabari Road, Netai Nagar, Kolkata, West Bengal 700099, India*

^f*Department of Physics, Ben-Gurion University, Beer-Sheva 84105, Israel*

^g*Department of Physics, Govt. Niranjan Kesharwani College, Kota, Bilaspur (C.G.)-495113, India*

^h*Department of Pure & Applied Physics, Guru Ghasidas Vishwavidyalaya (A Central University), Bilaspur (C.G.) - 495009, India*

ⁱ*Crimean Astrophysical Observatory, Russian Academy of Sciences, 298409, Nauchny, Crimea, Russia*

Abstract

We present Transit Timing Variations (TTVs) of HAT-P-12b, a low-density sub-Saturn mass planet orbiting a metal-poor K4 dwarf star. Using 14 years of observational data (2009-2022), our study incorporates 7 new ground-based photometric transit observations, three sectors of Transiting Exoplanet Survey Satellite (TESS) data, and 23 previously published light curves. A total of 46 light curves were analyzed using various analytical models, such as linear, orbital decay, apsidal precession, and sinusoidal models to investigate the presence of additional planets. The stellar tidal quality factor (Q'_* \sim 28.4)

Email addresses: kaviyasarathy1998@gmail.com (Kaviya Parthasarathy), shayna501@gapp.nthu.edu.tw (Hsin-Min Liu), jiang@phys.nthu.edu.tw (Ing-Guey Jiang), lichinyeh@mx.nthu.edu.tw (Li-Chin Yeh)

is lower than the theoretical predictions, making the orbital decay model an unlikely explanation. The apsidal precession model with a χ^2_r of 4.2 revealed a slight orbital eccentricity ($e = 0.0013$) and a precession rate of 0.0045 rad/epoch. Frequency analysis using the Generalized Lomb-Scargle (GLS) periodogram identified a significant periodic signal at 0.00415 cycles/day ($FAP = 5.1 \times 10^{-6} \%$), suggesting the influence of an additional planetary companion. The sinusoidal model provides the lowest reduced chi-squared value (χ^2_r) of 3.2. Sinusoidal fitting of the timing residuals estimated this companion to have a mass of approximately $0.02 M_J$, assuming it is in a 2:1 Mean-Motion Resonance (MMR) with HAT-P-12b. Additionally, the Applegate mechanism, with an amplitude much smaller than the observed TTV amplitude of 156 s, confirms that stellar activity is not responsible for the observed variations.

Keywords:

planetary systems, exoplanets: individual (HAT-P-12b), techniques: photometric

1. Introduction

Exoplanet research has transformed our understanding of planets beyond our solar system and has enhanced the quest for extraterrestrial life by identifying potentially habitable planets. As noted in the NASA Exoplanet Archive¹, approximately 6000 exoplanets had been identified through both ground-based and space-based telescopes by January 2025. Most of these discoveries have been made possible through observations of planetary transits and radial velocity (RV). Various dedicated space missions, including Kepler, K2, and TESS, and ground-based programs, including HATNet, SuperWASP, XO, and others, have contributed to the discovery (Bakos et al., 2004; McCullough et al., 2005; Pollacco et al., 2006; Borucki et al., 2011). A planetary transit occurs when a planet crosses in front of its host star, with its orbit nearly aligned with our line of sight. The resulting dip in the light curve allows us to determine the ratio of the planet's radius to that of the host star (R_p/R_\star), the semi-major axis (a), the orbital inclination (i), and the orbital period (P) from the interval between two consecutive transits (Mandel and Agol, 2002; Eastman et al., 2013). RV measurements of the

¹<https://exoplanetarchive.ipac.caltech.edu/>

host star allow us to ascertain the planet’s mass as well as the eccentricity of its orbit (Seager and Deming, 2010). Therefore, spectroscopic and photometric observations are essential for understanding the physical properties of the planetary system. Transit Timing Variations (TTVs) are an effective tool for detecting and characterizing exoplanetary systems. By examining minute deviations in the timing of a planet’s transit, we can deduce the existence of other planets or explore intricate orbital dynamics (Agol et al., 2005; Holman and Murray, 2005; Maciejewski et al., 2010; Jiang et al., 2013). These signals are particularly prominent in systems where planets are in or near Mean-Motion Resonances (MMR), facilitating precise measurements of the mass and orbital characteristics of the influencing planet. TTVs provides insights into orbital changes, such as orbital decay; occurs due to tidal dissipation between a planet and its host star, leading to a gradual decrease in the orbital period (Jiang et al., 2016; Yeh et al., 2024) and Apsidal Precession; changes in the orientation of a planet’s orbit over time due to gravitational interactions (Giménez and Bastero, 1995). Several authors investigated the theoretical predictions of TTVs (Maciejewski et al., 2016; Patra et al., 2017; Southworth et al., 2019; Mannaday et al., 2020; Yee et al., 2020; A-thano et al., 2022; Mannaday et al., 2022).

In 2006, HAT-P-12b was discovered using the HAT-5 telescope as part of the Hungarian Automated Telescope Network (Bakos et al., 2004). Subsequent photometric observations by Hartman et al. (2009) indicated that HAT-P-12b is a low-density warm sub-Saturn with a mass of $M_p = 0.211M_J$, a radius of $R_p = 0.959R_J$, and a density of $\rho_p = 0.0295 \text{ g cm}^{-3}$, with an orbital period of 3.21 days. It transits its host star, HAT-P-12, which is a relatively metal-poor K4 dwarf star with $[\text{Fe}/\text{H}] = -0.29$. The orbital and physical parameters of HAT-P-12 system have been refined by several studies (see for e.g., Mallonn et al. (2015); Lee et al. (2012); Alexoudi et al. (2018); Mancini et al. (2018)). The stellar and planetary parameters used in our studies are provided in Table 3. There have been no observed occultations of HAT-P-12b by its star (Todorov et al., 2013). Several authors investigated the atmospheric characteristics of HAT-P-12b. However, photometric examinations of HAT-P-12b have been confined to a limited studies, such as Öztürk and Erdem (2019); Sariya et al. (2021); Maciejewski et al. (2023). The studies of Öztürk and Erdem (2019); Maciejewski et al. (2023) discovered no evidence of a transiting planetary companion. However, Sariya et al. (2021) found non-sinusoidal TTVs in HAT-P-12b. Their two-planet model indicates the presence of a $0.2 M_J$ companion in an 8.8-day orbit. The contradict-

ing evidence emphasizes the necessity for additional inquiry. A long-term, high-precision monitoring effort is required to increase the accuracy of transit data.

In this paper, we introduce 7 newly observed ground-based transit lightcurves of HAT-P-12b collected across different epoch. These new observations are combined with, three sectors of Transiting Exoplanet Survey Satellite (TESS) and 23 publicly available lightcurves, spanning a total baseline of 14 years. We aim to determine whether the observed Transit Timing Variations(TTVs) of HAT-P-12b are caused by a planetary companion or by other factors.

Section 2 provides details on observations, data reduction techniques, and an overview of TESS data and light curves from the literature. Section 3 discusses the analysis of light curves to determine orbital parameters. The section 4 provides a detailed examination of TTVs using various models. The summary and concluding remark are provided in section 5.

Table 1: The observational record of HAT-P-12b.

Date	Epoch	Telescope	Filter	Duration of Exposure(s)	No. of Images	Transit Coverage
2012/06/01	580	WISE	R	20	218	Full
2014/04/17	793	P60	R	20	219	Full
2015/05/01	911	P60	R	30	146	Egress only
2015/06/15	925	P60	R	24	96	Egress only
2022/01/09	1672	TRT	R	30	331	Full
2022/02/07	1681	TRT	R	30	221	Ingress only
2022/05/08	1709	TRT	R	30	400	Full

2. Data

2.1. Ground-based observations

We conducted 7 new photometric observations of HAT-P-12b using three different telescopes:

1. The 60-inch telescope (P60) at Palomar Observatory, USA.
2. The 0.7m Thai Robotic Telescope at Sierra Remote Observations (TRT-SRO) in California, USA, equipped with an Andor iKon-M 934 CCD camera.
3. The 1m telescope at Wide Field Infrared Survey Explorer(WISE) Observatory, Israel.

The details of these observations, including the date, epoch, telescope used, filter type, and exposure times are summarized in Table 1.

2.2. Data reductions

The raw CCD images from the three telescopes were processed using IRAF² software for data reduction. The reduction process begins with bias correction, dark correction, and flat-field correction and calibrated for photometric analysis. Aperture photometry was performed using the IRAF phot package. Aperture sizes were optimized based on the seeing conditions to maximize the signal-to-noise ratio. Two or three comparison stars, with a magnitude similar to HAT-P-12 were visually inspected and chosen. The `txt_dump` task was used to extract the results of aperture photometry which are the times, fluxes, and magnitude measurements of the target star and the comparison stars. The BJD_{TDB} , relative flux, and its errors were used to generate light curves. Relative flux and its associated errors were calculated based on the flux and magnitude values of the target and the comparison stars provided by IRAF. The observation times were converted to Barycentric Julian Date in Barycentric Dynamical Time (BJD_{TDB}) using an online tool³ developed by Eastman et al. (2010). The normalized light curves and their residuals obtained from our observations are illustrated in Figure 1. The normalized light curves can be accessed through a machine-readable format shown in Table 2.

2.3. Transiting exoplanet survey satellite (TESS)

TESS observed HAT-P-12 in sectors 23,49 and 50 covering 16 transits. We retrieved the Photometric data of these sectors, which are the times, fluxes, and errors from the Mikulski Archive for Space Telescope (MAST)⁴ using JULIET package (Espinoza et al., 2019). Sector 23 contains 6 transits covering from 2020/03/24 to 2020/04/12. Sector 49 contains 5 transits covering from 2022/03/04 to 2022/03/23. Sector 50 contains 5 transits covering from 2022/04/02 to 2022/04/18. Each transit observed by TESS provided over 3,000 data points. To determine the mid-transit time, we only require the

²IRAF is distributed by the National Optical Astronomy Observatories, which are operated by the Association of Universities for Research in Astronomy, Inc., under a cooperative agreement with the National Science Foundation.<http://iraf.noao.edu/>

³<https://astroutils.astronomy.osu.edu/time/utc2bjd.html>

⁴<http://mast.stsci.edu>

Table 2: The normalized light curves of HAT-P-12b obtained by our ground-based observations and TESS. A small portion is shown here. The entire table is available in the machine-readable form.

Epoch	BJD_{TDB}	Normalized Flux	Uncertainty
580	2456080.241507	1.00751	0.00394
	2456080.242333	1.00402	0.00392
	2456080.243159	1.01152	0.00395
	2456080.243983	1.00774	0.00394
	2456080.244808	1.00641	0.00393

793	2456764.676953	1.01611	0.00281
	2456764.677480	1.01836	0.00281
	2456764.678005	1.02127	0.00282
	2456764.678529	1.01788	0.00281
	2456764.679055	1.01889	0.00282

911	2457143.848503	0.99631	0.00275
	2457143.849147	0.99596	0.00318
	2457143.849808	0.99908	0.00319
	2457143.850452	0.99957	0.00319
	2457143.851097	0.99809	0.00379

transit portion of the light curve, therefore the out-of-transit baseline which primarily contains noise and stellar Variability was manually removed. The processed light curves for all 16 transits observed by TESS are presented in Figure 2 and the values are available in the machine-readable format shown in Table 2.

2.4. Literature data

This work utilizes a total of 23 publicly available light curves (Hartman et al. (2009),Lee et al. (2012),Mallonn et al. (2015),Alexoudi et al. (2018),Sariya et al. (2021)). The light curves are analyzed using the same method as our observation data (refer section 3) to reconfirm their mid-transit times.

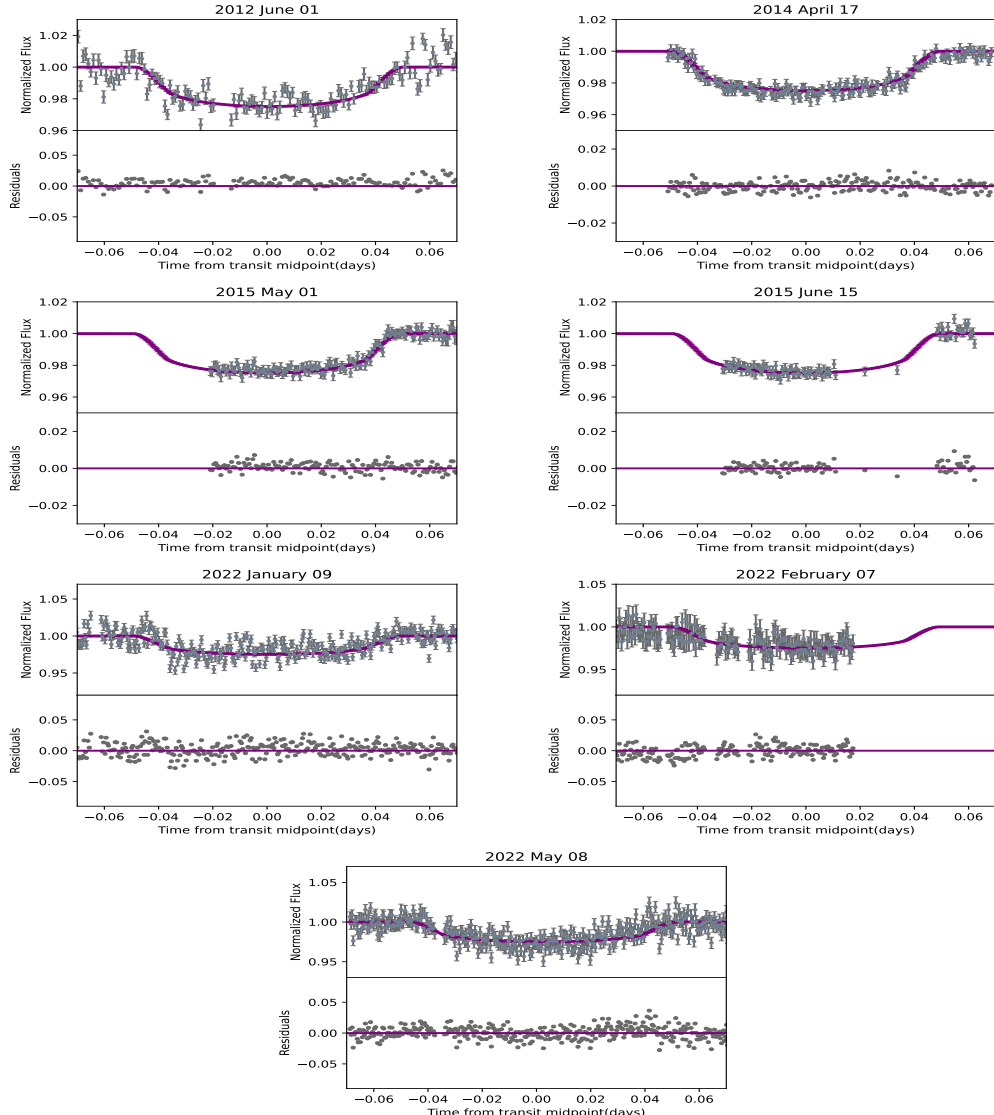


Figure 1: Ground-based transit light curves of HAT-P-12b from various observation epochs. The solid lines represent the best-fit models, and the residuals are shown below each light curve.

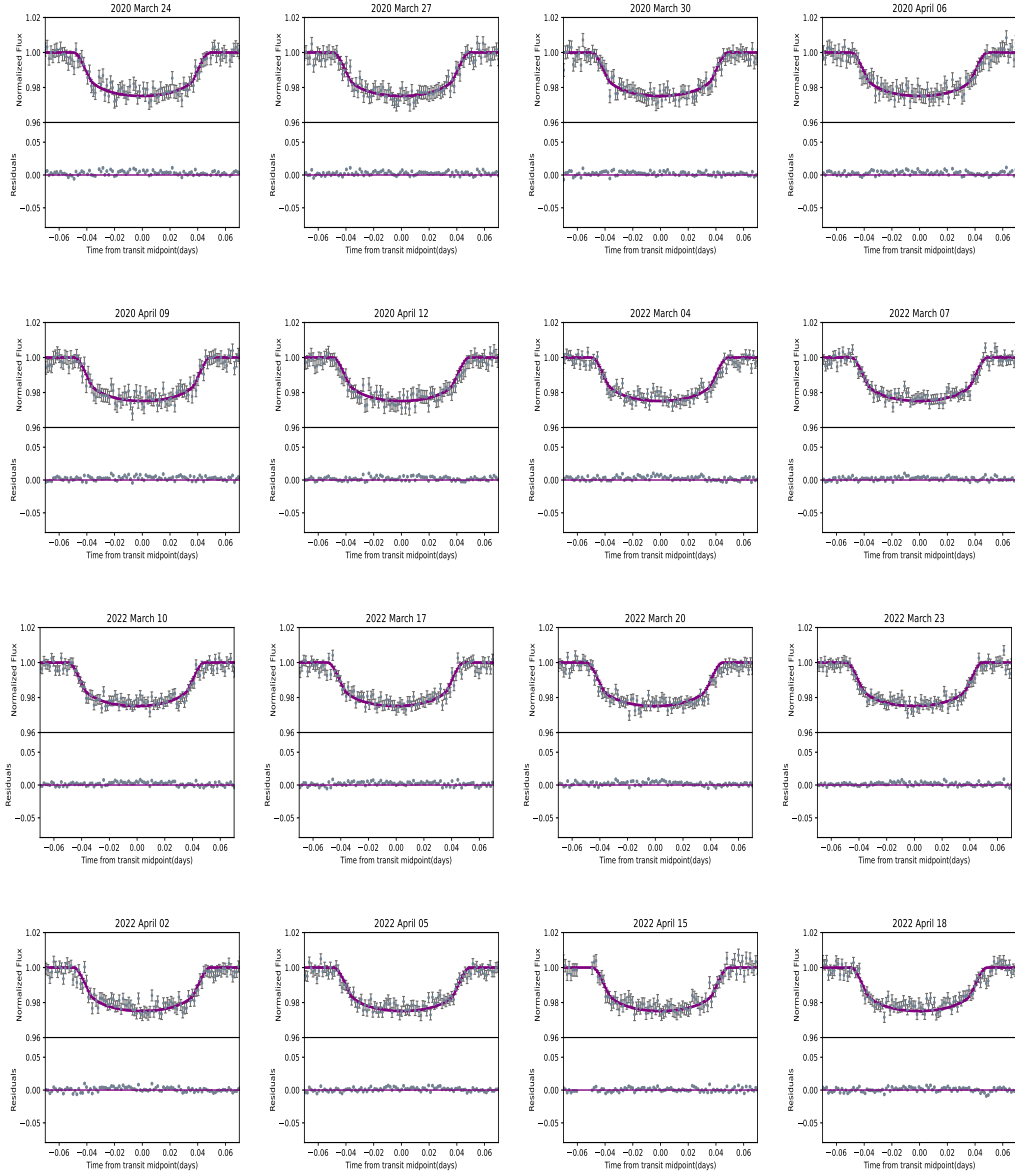


Figure 2: Space-based transit light curves of HAT-P-12b from different sectors of TESS. The solid lines represent the best-fit models, and the residuals are shown below each light curve.

3. Light Curve Analysis

The orbital and planetary parameters of HAT-P-12b were derived using the Python package `pylightcurve`, specifically designed for modeling and analyzing light curves. A total of 46 light curves were modeled individually. `pylightcurve` utilizes the Exoplanet Characterisation Catalogue(ECC), developed as part of the Exoclock Project (Kokori et al., 2022). This ECC catalog contains information on more than 370 exoplanets including HAT-P-12b. Access to the data is facilitated by the `pylightcurve.get_planet()` function, which provides all the necessary parameters and its initial corresponding values for modeling light curves. The adopted stellar and planetary parameters are listed in Table 3.

Table 3: Stellar and planetary parameters of HAT-P-12b used in our work. The parameters are adopted from (Hartman et al., 2009).

Parameter	Value
Stellar Parameters	
$M_*(M_\odot)$	0.733 ± 0.018
$R_*(R_\odot)$	$0.701^{+0.017}_{-0.012}$
$\log g$ (cgs)	4.61 ± 0.01
[Fe/H]	-0.29 ± 0.05
T_{eff} (K)	4650 ± 60
V (mag)	12.84
Planetary Parameters	
$M_p(M_J)$	0.211 ± 0.012
$R_p(R_J)$	$0.959^{+0.029}_{-0.021}$
a (AU)	0.0384 ± 0.0003
ρ_p (g cm $^{-3}$)	0.0295 ± 0.025

The planetary parameters used by `pylightcurve` for modeling light curves include orbital period P in days, epoch of mid-transit T_0 in BJD, orbital inclination i in degrees, eccentricity e , semi-major axes a in the units of stellar radius R_* , radius of the Planet R_p in the units of stellar radius R_* , an argument of periastron ω . while fitting, the orbital period and eccentricity were treated as fixed parameters. The orbital period was fixed to enable the detection of TTVs, allowing for any observed deviations in transit timing. The eccentricity was fixed, based on the assumption that the orbit of HAT-P-12b

is circular. The remaining orbital parameters t_0 , i , a are set as free parameters. The parameter setting and the corresponding values used as inputs for modeling light curves are shown in Table 4.

The light curve fitting process was performed using the planet-transit-fitting function in `pylightcurve`, which employs an *emcee* Markov Chain Monte Carlo (MCMC) (Foreman-Mackey et al., 2013) sampler to perform simultaneous detrending and normalization of the light curves. For detrending, a first-order polynomial function was applied to remove the linear trends in the baseline. The default configuration of this function, involves 130,000 steps, 200 walkers, and 30,000 burn-in steps. This gives adequate convergence of the chains and parameter exploration, providing posterior probability distributions. A quadratic limb-darkening method was adopted to characterize the stellar limb-darkening effect. The filters used for observation and their associated limb darkening coefficients(u_1, u_2), are shown in Table 5. The overall fitting results are presented in Table 6.

Table 4: The initial values and setting of planetary parameters used by the fitting processes of `pylightcurve`.

Parameters	Initial Values	Priors	Prior Distribution
P (days)	3.21305762	–	Fixed
$T_0(\text{BJD}_{TDB})$	2456851.481119	[−0.2, 0.2]	Uniform
i (deg)	89.0	[70.0, 90.0]	Uniform
a/R_\star	11.77	[0.5, 2.0]	Uniform
R_p/R_\star	0.1406	[0.5, 2.0]	Uniform
e	0.0	–	Fixed
ω (deg)	0.0	–	Fixed

4. Transit Timing Analysis

We analyzed the TTVs of HAT-P-12b using our modeled 46 light curves. To investigate potential deviations from a strictly periodic transit pattern, we adopted three models: the linear model, the orbital decay model, and the Apsidal Precession model followed Patra et al. (2017); Yee et al. (2020)

4.1. Linear model

The linear model assumes a circular orbit with a constant orbital period. We derived a new ephemeris for HAT-P-12b by fitting a linear model,

Table 5: The limb darkening coefficients of HAT-P-12b adopted from `pylightcurve`.

Filter	u_1	u_2
B	0.93739	-0.07324
R	0.59585	0.11564
I	0.47749	0.13526
g'	0.87745	-0.03303
r'	0.62543	0.11007
z'	0.41697	0.14313
TESS	0.48727	0.13392

$$T_m^c(E) = T_0 + EP, \quad (1)$$

where $T_m^c(E)$ is the calculated mid-transit time at epoch E , T_0 is the reference mid-transit time, P is the orbital period, and E denotes the integer epoch number. The first observed transit of HAT-P-12b is assigned $E = 0$.

We used the *emcee* Monte Carlo Markov Chain (MCMC) sampler (Foreman-Mackey et al., 2013) to fit the observed mid-transit times to the linear model. We used 50 walkers and 10^6 steps for this analysis to sample the posterior probability distributions. The initial 10^3 burn-in steps were discarded to ensure that the chains had to converge. We considered uniform distributions as priors for the free parameters.

The best-fit values of the model parameters derived from the MCMC Posterior probability distribution are: $P = 3.213059$ days and $T_0 = 2454216.77325$ (BJD_{TDB}). The resultant uniform uncertainties at one sigma are given in Table 7. Since the number of dimensions for the linear model is 2, the reduced chi-square χ_{red}^2 with 44 degrees of freedom is 8.1. The high χ_{red}^2 suggests possible deviations from strict periodicity.

4.2. Orbital decay model

The second model assumes a circular orbit and the period is changing at a steady rate.

$$T_d^c(E) = T_{d0} + EP_d + \frac{1}{2} \frac{dP_d}{dE} E^2, \quad (2)$$

where $T_d^c(E)$ is the calculated mid-transit time, T_{d0} is the mid-transit time at $E = 0$, E is the epoch number, P_d is the orbital period, $\frac{dP_d}{dE}$ is the change

Table 6: Fitting results obtained from `pylightcurve`

Epoch	$Tm(BJD_{TDB} - 2450000)$ (days)	Avg err	O-C(days)	$i(^{\circ})$	r_p/r_*	a/r_*	source
0	4216.77273 ^{+0.00035} _{-0.0019}	0.001125	-0.00053	88.9 ^{+0.71} _{-0.19}	11.95 ^{+0.08} _{-0.20}	0.1399 ^{+0.0011} _{-0.0010}	(a)
203	4869.02361 ^{+0.00022} _{-0.00015}	0.00019	-0.00063	89.1 ^{+0.5} _{-1.0}	11.74 ^{+0.14} _{-0.68}	0.143 ^{+0.0026} _{-0.0017}	(a)
212	4897.94230 ^{+0.00033} _{-0.00022}	0.00028	0.00053	88.9 ^{+0.7} _{-0.4}	12.39 ^{+0.12} _{-0.34}	0.137 ^{+0.0010} _{-0.0018}	(a)
342	5315.63826 ^{+0.00053} _{-0.00024}	0.00039	-0.00118	89.1 ^{+0.3} _{-0.3}	11.75 ^{+0.37} _{-0.18}	0.138 ^{+0.0020} _{-0.0023}	(c)
346	5328.4924 ^{+0.0005} _{-0.0009}	0.0007	0.00072	88.9 ^{+0.7} _{-0.4}	11.93 ^{+0.13} _{-0.26}	0.1368 ^{+0.0021} _{-0.0008}	(c)
446	5649.79768 ^{+0.00024} _{-0.00018}	0.00021	0.00010	89.1 ^{+0.6} _{-0.4}	11.68 ^{+0.09} _{-0.23}	0.1373 ^{+0.0018} _{-0.0009}	(d)
451	5665.8624 ^{+0.0010} _{-0.0015}	0.0008	-0.00048	89.0 ^{+0.6} _{-0.6}	12.05 ^{+0.13} _{-0.48}	0.142 ^{+0.0029} _{-0.0012}	(d)
455	5678.7139 ^{+0.0003} _{-0.0004}	0.0004	-0.00121	89.1 ^{+0.7} _{-0.3}	11.91 ^{+0.12} _{-0.32}	0.135 ^{+0.0018} _{-0.0011}	(e)
460	5694.7808 ^{+0.0003} _{-0.0004}	0.0004	0.00039	89.1 ^{+0.7} _{-0.3}	11.88 ^{+0.10} _{-0.17}	0.1402 ^{+0.0012} _{-0.0009}	(d)
567	6038.5774 ^{+0.0009} _{-0.0006}	0.0008	-0.00032	89.0 ^{+0.8} _{-0.7}	11.8 ^{+2.9} _{-0.7}	0.124 ^{+0.013} _{-0.007}	(c)
580	6038.5774 ^{+0.0008} _{-0.0003}	0.0006	-0.00089	89.0 ^{+0.7} _{-0.8}	11.2 ^{+0.3} _{-0.5}	0.143 ^{+0.0028} _{-0.0019}	(g)
698	6459.48784 ^{+0.0027} _{-0.0024}	0.00026	-0.00061	89.0 ^{+0.6} _{-0.5}	11.79 ^{+0.14} _{-0.35}	0.136 ^{+0.0018} _{-0.0010}	(c)
783	6732.59740 ^{+0.00025} _{-0.00020}	0.00023	-0.00107	89.73 ^{+0.20} _{-0.45}	11.85 ^{+0.07} _{-0.11}	0.137 ^{+0.0007} _{-0.0007}	(c)
784	6732.59740 ^{+0.0014} _{-0.0004}	0.0009	-0.00133	89.1 ^{+0.7} _{-0.5}	12.04 ^{+0.17} _{-0.30}	0.130 ^{+0.006} _{-0.003}	(e)
792	6761.51607 ^{+0.00014} _{-0.00018}	0.00016	0.00007	89.77 ^{+0.18} _{-0.59}	11.91 ^{+0.06} _{-0.14}	0.140 ^{+0.0007} _{-0.0005}	(c)
793	6732.59740 ^{+0.0005} _{-0.0006}	0.0006	-0.00126	88.9 ^{+0.7} _{-0.5}	12.02 ^{+0.18} _{-0.33}	0.137 ^{+0.0004} _{-0.0004}	(g)
911	7143.8694 ^{+0.0006} _{-0.0006}	0.0006	-0.00062	88.9 ^{+0.8} _{-1.5}	11.8 ^{+1.2} _{-1.1}	0.140 ^{+0.0008} _{-0.0003}	(g)
925	7188.8515 ^{+0.0027} _{-0.0018}	0.0023	-0.00135	89.6 ^{+0.4} _{-1.4}	11.5 ^{+0.6} _{-0.8}	0.1415 ^{+0.0039} _{-0.0019}	(g)
928	7188.8515 ^{+0.0023} _{-0.0006}	0.0015	-0.00083	89.0 ^{+0.6} _{-0.5}	11.94 ^{+0.15} _{-0.29}	0.145 ^{+0.003} _{-0.003}	(c)
934	7217.7697 ^{+0.0008} _{-0.0005}	0.0007	-0.00068	89.0 ^{+0.7} _{-0.9}	11.9 ^{+0.4} _{-0.6}	0.137 ^{+0.0027} _{-0.0018}	(e)
1027	7516.58666 ^{+0.0011} _{-0.00021}	0.000655	0.00179	88.8 ^{+0.8} _{-0.2}	11.79 ^{+0.14} _{-0.39}	0.1377 ^{+0.0026} _{-0.0020}	(b)
1045	7574.4189 ^{+0.0003} _{-0.0003}	0.0003	-0.00103	89.0 ^{+0.4} _{-0.6}	12.08 ^{+0.13} _{-0.49}	0.1402 ^{+0.0013} _{-0.0013}	(c)
1126	7574.4189 ^{+0.0005} _{-0.0008}	0.0007	0.00169	88.9 ^{+0.8} _{-0.7}	12.05 ^{+0.20} _{-0.49}	0.134 ^{+0.0040} _{-0.0014}	(b)
1139	7876.4478 ^{+0.0003} _{-0.0003}	0.0003	0.00032	88.9 ^{+0.7} _{-0.4}	11.83 ^{+0.11} _{-0.28}	0.139 ^{+0.0020} _{-0.0010}	(b)
1140	7879.66428 ^{+0.00024} _{-0.00028}	0.00026	0.00374	89.3 ^{+0.6} _{-1.4}	11.57 ^{+0.22} _{-0.81}	0.143 ^{+0.0060} _{-0.0015}	(b)
1144	7892.51414 ^{+0.00010} _{-0.00013}	0.00012	0.00136	88.9 ^{+0.59} _{-0.22}	11.81 ^{+0.17} _{-0.15}	0.1375 ^{+0.0029} _{-0.0005}	(b)
1159	7940.7071 ^{+0.003} _{-0.004}	0.0017	-0.00156	89.0 ^{+0.6} _{-1.3}	11.83 ^{+0.18} _{-0.88}	0.139 ^{+0.005} _{-0.003}	(b)
1468	7940.7071 ^{+0.0009} _{-0.0006}	0.0008	-0.00110	88.8 ^{+0.8} _{-1.1}	11.7 ^{+0.4} _{-0.8}	0.1358 ^{+0.0040} _{-0.0022}	(f)
1469	8936.7555 ^{+0.0009} _{-0.0004}	0.0007	-0.00146	89.0 ^{+0.8} _{-1.5}	11.8 ^{+0.4} _{-1.0}	0.1406 ^{+0.0048} _{-0.0017}	(f)
1470	8936.7555 ^{+0.0009} _{-0.0004}	0.0007	-0.00102	88.9 ^{+0.7} _{-1.0}	12.1 ^{+0.3} _{-0.7}	0.1382 ^{+0.0035} _{-0.0018}	(f)
1472	8936.7555 ^{+0.0008} _{-0.0007}	0.0008	-0.00133	89.0 ^{+0.8} _{-1.9}	11.72 ^{+0.23} _{-1.25}	0.139 ^{+0.003} _{-0.003}	(f)
1473	8949.6075 ^{+0.0008} _{-0.0005}	0.0007	-0.00169	88.9 ^{+0.7} _{-1.0}	11.8 ^{+0.4} _{-0.6}	0.1373 ^{+0.0018} _{-0.0018}	(f)
1474	8952.8210 ^{+0.0007} _{-0.0006}	0.0007	-0.00125	89.0 ^{+0.7} _{-1.2}	11.6 ^{+0.24} _{-0.87}	0.1383 ^{+0.0038} _{-0.0019}	(f)
1672	9589.0063 ^{+0.0007} _{-0.0005}	0.0006	-0.00164	89.7 ^{+0.22} _{-0.75}	12.29 ^{+0.22} _{-0.39}	0.145 ^{+0.004} _{-0.005}	(g)
1681	9617.9237 ^{+0.0046} _{-0.0023}	0.0035	-0.00177	88.9 ^{+0.8} _{-1.2}	11.7 ^{+3.0} _{-1.0}	0.139 ^{+0.0043} _{-0.0043}	(g)
1689	9643.6288 ^{+0.0007} _{-0.0003}	0.0005	-0.00114	88.9 ^{+0.7} _{-0.6}	11.75 ^{+0.15} _{-0.42}	0.136 ^{+0.0024} _{-0.0016}	(f)
1690	9646.8415 ^{+0.0005} _{-0.0005}	0.0005	-0.00150	89.0 ^{+0.7} _{-0.6}	11.93 ^{+0.20} _{-0.37}	0.1360 ^{+0.0025} _{-0.0016}	(f)
1691	9646.8415 ^{+0.0005} _{-0.0006}	0.0006	-0.00126	89.0 ^{+0.7} _{-0.8}	11.89 ^{+0.23} _{-0.45}	0.1345 ^{+0.0028} _{-0.0014}	(f)
1693	9646.8415 ^{+0.0006} _{-0.0005}	0.0006	-0.00148	89.0 ^{+0.7} _{-0.7}	12.08 ^{+0.20} _{-0.50}	0.1348 ^{+0.0030} _{-0.0015}	(f)
1694	9659.6940 ^{+0.0006} _{-0.0004}	0.0005	-0.00124	89.0 ^{+0.7} _{-0.8}	11.66 ^{+0.19} _{-0.54}	0.136 ^{+0.0024} _{-0.0007}	(f)
1695	9662.9063 ^{+0.0005} _{-0.0005}	0.0005	-0.00179	89.0 ^{+0.7} _{-0.8}	11.86 ^{+0.21} _{-0.46}	0.1370 ^{+0.0024} _{-0.0016}	(f)
1698	9672.5460 ^{+0.0007} _{-0.0005}	0.0006	-0.00147	89.0 ^{+0.7} _{-1.3}	11.8 ^{+0.3} _{-0.8}	0.135 ^{+0.0033} _{-0.0022}	(f)
1699	9672.5460 ^{+0.0007} _{-0.0006}	0.0007	-0.00223	89.1 ^{+0.8} _{-1.0}	11.8 ^{+0.3} _{-1.0}	0.136 ^{+0.0038} _{-0.0021}	(f)
1702	9685.3979 ^{+0.0006} _{-0.0005}	0.0006	-0.00181	89.0 ^{+0.7} _{-0.7}	11.79 ^{+0.21} _{-0.42}	0.1406 ^{+0.0028} _{-0.0014}	(f)
1703	9688.6115 ^{+0.0006} _{-0.0008}	0.0007	-0.00127	88.9 ^{+0.3} _{-1.6}	11.8 ^{+0.3} _{-1.6}	0.137 ^{+0.0058} _{-0.0015}	(f)
1709	9688.6115 ^{+0.0020} _{-0.0007}	0.0014	-0.00412	85.7 ^{+1.6} _{-0.3}	10.4 ^{+1.5} _{-0.5}	0.158 ^{+0.006} _{-0.010}	(g)

(a)Hartman et al. (2009), (b)Alexoudi et al. (2018), (c)Mancini et al.

(2018),(d)Lee et al. (2012),(e)Sariya et al. (2021), (f)TESS,(g)our study

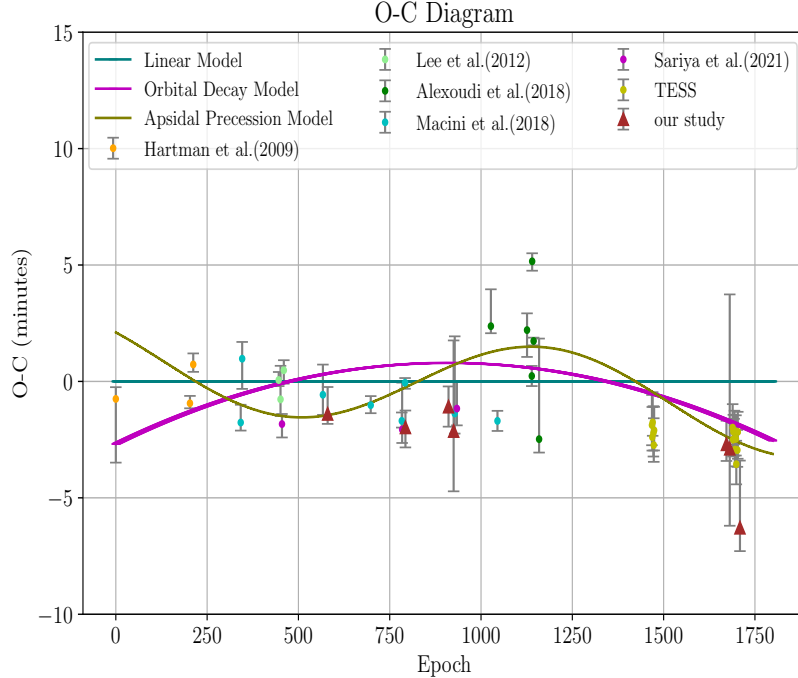


Figure 3: Transit Timing Variation (TTV) diagram for HAT-P-12b after subtracting the linear model. The plot compares the observed-minus-calculated (O-C) values against linear, orbital decay, and apsidal precession models

of the orbital period in each orbit. Similar to the linear model, we used an emcee MCMC sampler to fit the orbital decay model.

The best-fit values of the parameters from the Posterior probability distribution are $P = 3.213064$ days, $T_0 = 2454216.77138$ (BJD_{TDB}), and $\frac{dP_d}{dE} = -5.85^{+0.64}_{-0.63} \times 10^{-9}$ (days/orbit) or -0.051 ± 0.006 seconds. The uncertainty of these parameters at one sigma is given in Table 7.

The χ^2_{red} of the model with 43 degrees of freedom is 6.3 which is lower than the linear model.

4.2.1. Stellar tidal quality

The stellar tidal quality Q'_* can be expressed as (Maciejewski et al., 2018):

$$Q'_\star = -\frac{27}{2}\pi\left(\frac{M_p}{M_\star}\right)\left(\frac{a}{R_\star}\right)^{-5}\left(\frac{dP_d}{dE}\right)^{-1}P, \quad (3)$$

where the value of M_p , M_\star and a/R_\star are taken from Hartman et al. (2009). The value of dP_d/dE is taken from our decay model fitting. Using these values the value of Q'_\star is calculated as 28.4, a significantly lower value compared to the theoretical predictions. The study by Penev et al. (2018) analyzed a sample of 188 known hot Jupiters with an orbital period < 3.5 days and $T_{eff} < 6100$ k. Their analysis estimated the value $10^5 \leq Q'_\star \leq 10^7$. This low Q'_\star value suggests that there must be other dynamics happening in the HAT-P-12 system that cannot be explained by the decay model. To investigate further, we choose an apsidal model for possible explanations.

4.3. Apsidal model

The apsidal model assumes that the planetary orbit is slightly eccentric and its argument of pericenter is precessing uniformly over time Wolf and Ragozzine (2009). We adopted the apsidal model from Giménez and Bastero (1995),

$$T_{ap}^c(E) = T_{ap0} + P_s E - \frac{e P_s \cos(\omega_0 + E \frac{dw}{dE})}{\pi(1 - \frac{dw}{2\pi})}, \quad (4)$$

where T_{ap0} is the reference time, e is the eccentricity, ω is the argument of pericenter and P_s is the sideral period and $\frac{dw}{dE}$. This model has five free parameters: T_{ap0} , P_s , e , ω , and $\frac{dw}{dE}$. To fit this model, we used the same MCMC sampler described for the linear model in Section 4.1. The best-fit values of the parameters, obtained from the Posterior probability distribution are: $P = 3.213064$ days, $T_0 = 2454216.77393$ (BJD_{TDB}), $e = 0.00130$, $\omega_0 = 4.09$ rad and $\frac{dw}{dE} = 0.0045$ rad/epoch. The results of the fitted parameters with relative uncertainties are listed in the Table 7. The χ^2_{red} of the model with 43 degrees of freedom is 4.2 which is better than the linear and decay model.

4.4. Model selection

The Akaike Information Criterion (AIC) and Bayesian Information Criterion (BIC) are commonly used statistical measures to determine the best model.

$$AIC = \chi^2 + 2k, \quad (5)$$

$$BIC = \chi^2 + k \ln(n), \quad (6)$$

where k represents the number of free parameters and n denotes the number of data points. In this case, $n = 46, k = 2$ for linear model, $k = 3$ for decay model, $k = 5$ for apsidal model. The AIC values of the linear, decay and apsidal models are 361.19, 279.71 and 185.96 respectively. Likewise, the BIC values for the linear, decay, and apsidal models are 364.85, 285.19, and 195.11. The difference in BIC between the apsidal and decay model Δ_{BIC} is 45.04. Similarly, the AIC favours the decay model by Δ_{AIC} is 46.87. To identify the most appropriate model, χ^2_{red} and the AIC/BIC of the three models were analyzed and compared. Among these, the apsidal model indicates the lowest χ^2_{red} value (3.1) and the lowest AIC/BIC value which strongly favored as the most appropriate representation of the system. The best-fit values of the three models, χ^2_{red} , AIC/BIC are presented in Table 7. The timing residuals for the orbital decay model were obtained by subtracting the mid-transit time calculated using a linear model. Similarly, the apsidal model was obtained by subtracting from the linear model mid-transit times. The resulting Observed-Calculated (O-C) values as a function of an epoch are illustrated in Figure 3.

4.5. Sinusoidal model

To explore the possibility of additional planets affecting the Transit times of HAT-P-12b, we analyzed the observed TTVs using the Generalized Lomb-Scargle (GLS) Periodogram (Lomb, 1976; Scargle, 1982). This method is particularly well-suited for analyzing unevenly spaced time series data, which is common in transit observations. It offers the advantage of incorporating uncertainties, thereby improving the robustness of the frequency analysis (Zechmeister and Kürster, 2009). We used the GLSP code provided by the *PyAstronomy*⁵ package. The default normalization Zechmeister & Kurster (ZK) was used for normalization. The resulting periodogram shown in Figure 4 exhibited multiple peaks of nearly the same height. We used *find_peaks* from the *scipy*⁶ package to find the top five prominent peaks and labeled as f_1 to f_5 and consider their false alarm probability (FAP) to check their significance. The frequency of each peak and their FAP values are summarized

⁵<https://github.com/sczesla/PyAstronomy>

⁶https://docs.scipy.org/doc/scipy/reference/generated/scipy.signal.find_peaks.html

Table 7: The Uniform Priors and Best-fit Parameters for HAT-P-12b

Model	Best-fit Values
Linear model	
$P[\text{days}]$	$3.213059^{+1.5 \times 10^{-7}}_{-1.5 \times 10^{-7}}$
$T_0[BJD_{TDB} - 2450000]$	$4216.77325^{+0.00017}_{-0.00017}$
χ^2_r	8.1
AIC/BIC	361/364
Orbital decay model	
$P_d[\text{days}]$	$3.213064^{+6.04 \times 10^{-7}}_{-6.04 \times 10^{-7}}$
$T_0[BJD_{TDB} - 2450000]$	$4216.77138^{+0.00029}_{-0.00028}$
dP/dE[seconds]	-0.051 ± 0.006
χ^2_r	6.3
AIC/BIC	279/285
Apsidal model	
$P_s[\text{days}]$	$3.213058^{+3.8 \times 10^{-7}}_{-3.8 \times 10^{-7}}$
$T_0[BJD_{TDB} - 2450000]$	$4216.77393^{+0.0009}_{-0.0004}$
e	$0.00130^{+0.0001}_{-0.0001}$
$\omega_0[\text{rad}]$	$4.095^{+0.38}_{-0.36}$
dw/dE[rad/epoch]	$0.0045^{+0.0004}_{-0.0004}$
χ^2_r	4.2
AIC/BIC	185/195

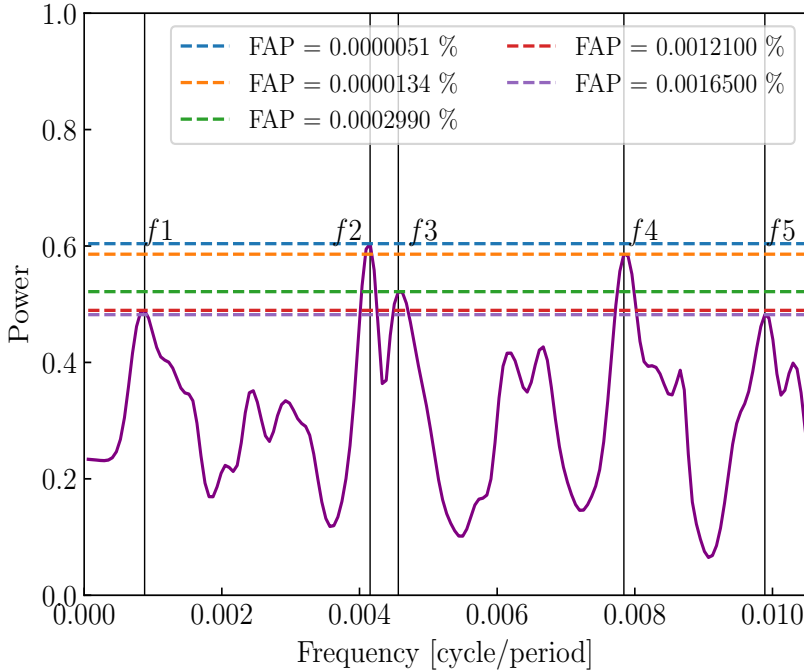


Figure 4: Generalized Lomb-Scargle periodogram of HAT-P-12b TTV data, indicating periodic signals and their false alarm probability (FAP) levels. Peaks are annotated with their frequencies(f1 to f5)

in Table 8. To evaluate these peaks further, we fit each one with a sinusoidal model given by von Essen et al. (2019),

$$TTVs(E) = A_{TTVs} \sin(2\pi f E - \phi), \quad (7)$$

where A_{TTVs} is the amplitude of TTV in minutes, E is the epoch, and ϕ is the phase, f is the frequency. For each frequency value obtained from the GLS periodogram, the sinusoidal fitting was performed and we estimated the values for ϕ and A_{TTVs} . We calculated the χ^2_R and BIC for these fits to choose the best frequency. The peak at $f_2 = 0.00415$ cycles/day had the lowest values of $\chi^2_r = 3.2$, $BIC = 149.3$ and lowest $FAP = 0.5 \times 10^{-5}$. The amplitude of the best frequency is A_{TTV} is 2.6 minutes. The FAPs, along with the amplitude, phase, χ^2_r , and BIC values for each frequency f1-f5 are presented in Table 8. Our timing residuals(O-C) clearly show the sinusoidal pattern, which

Table 8: Frequency values of sinusoidal model

No.of frequency	frequency (cycle/period)	FAP	A_{TTV} (minutes)	Phase	χ^2_r	BIC
f1	0.00087	0.00121	1.64 $^{+0.12}_{-0.12}$	1.49 $^{+0.09}_{-0.09}$	4.21	193.0
f2	0.00415	0.000005	2.62 $^{+0.19}_{-0.19}$	2.11 $^{+0.04}_{-0.05}$	3.22	149.3
f3	0.00456	0.000299	1.80 $^{+0.13}_{-0.14}$	0.162 $^{+0.08}_{-0.08}$	3.90	179.3
f4	0.00784	0.0000134	2.15 $^{+0.17}_{-0.18}$	0.76 $^{+0.06}_{-0.06}$	3.36	155.5
f5	0.00988	0.00165	1.75 $^{+0.14}_{-0.15}$	0.13 $^{+0.10}_{-0.10}$	4.26	195.4

indicates the presence of periodic signal are shown in Figure 5. This strongly suggests the influence of an additional planet in the system. The sinusoidal fitting allowed us to estimate the parameters of the additional planet. In our next section, we aim to find the mass and period of the candidate planet.

4.6. Mass of an additional planet

To estimate the mass of the perturbing planet, we employed the analytical model of Lithwick et al. (2012) which relates the TTV amplitude (V) to the orbital period, μ is the mass of outer planet, and j is the resonance.

$$V = P \frac{\mu}{\pi j^{2/3} (j-1)^{1/3} \Delta} \left(-f - \frac{3}{2} \frac{Z_{free}^*}{\Delta} \right), \quad (8)$$

where $\Delta = \frac{P'}{P} \frac{j}{j-1} - 1$, represents the normalized distance from resonance, f is the Laplace coefficients, Z_{free}^* is the free eccentricity, respectively. We assume that the perturber planet is in a 2:1 MMR $j:j-1$ with HAT-P-12b and both planets have circular orbits, i.e. $Z_{free}^* = 0$.

Using the TTV amplitude found from our sinusoidal model ($V=2.6$ minutes) and the known orbital period (P) of HAT-P-12b we estimated the perturbing planet's mass to be approximately $0.02 M_J$ and its orbital period to be approximately 6.24 days.

4.7. Applegate mechanism

We examined the Applegate mechanism to determine whether the observed TTVs in the HAT-P-12 system could result from stellar activity (Applegate, 1992). The stellar activities of 59 systems including HAT-P-12b were analyzed by Watson and Marsh (2010) and found that the amplitude of the Applegate effect over 11, 22, and 50-year timescales. They found that for

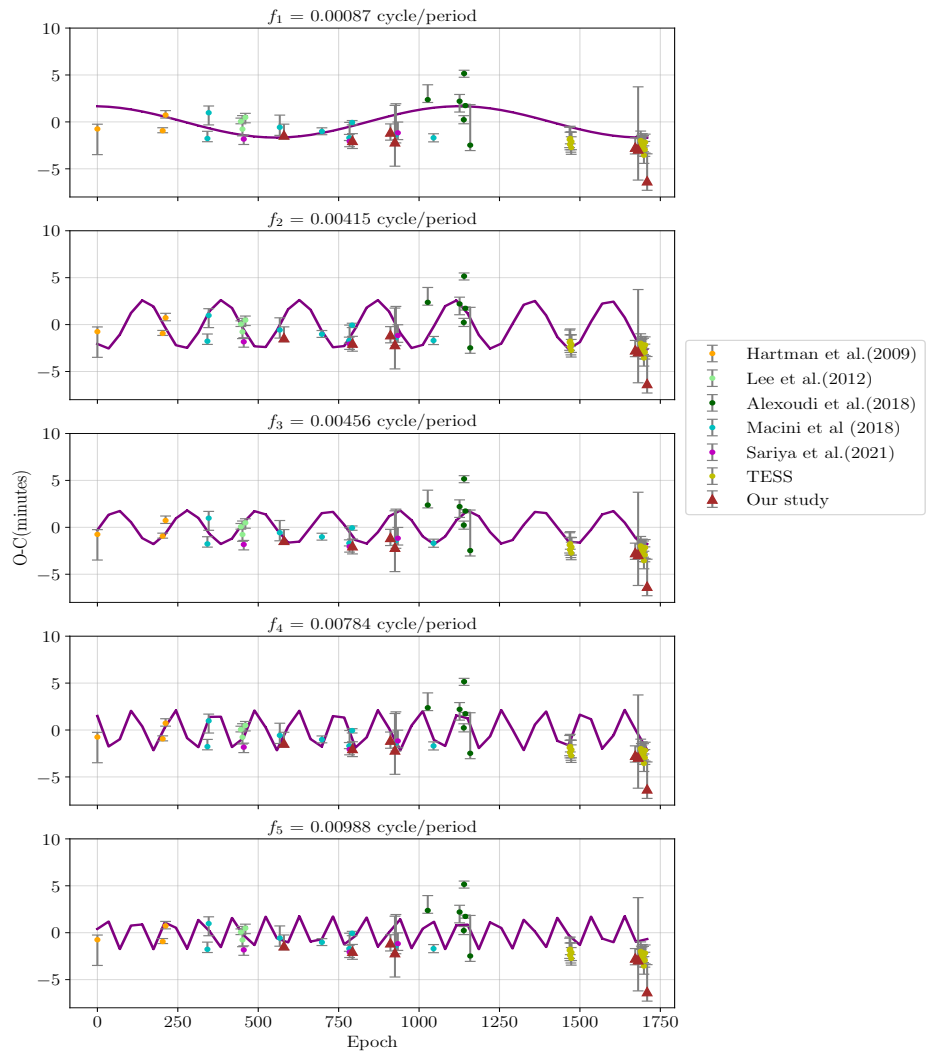


Figure 5: Sinusoidal model fitting for the most significant frequencies identified in the GLS periodogram analysis.

HAT-P-12b, $\delta t_{50} = 0.4$ s. However, our observed TTV amplitude found using the sinusoidal model with the frequency f_2 (see section 4.5) is 156 seconds, significantly larger than the amplitude of the Applegate effect.

The variations due to the Applegate mechanism are at best quasiperiodic, while the TTVs caused by an additional planet in a mean-motion resonance orbit generally have strictly periodic and larger transit-time variations. It is obvious that our observed TTVs exhibit sinusoidal variations as shown in Figure 5. Therefore Applegate mechanism may not be the possible cause of TTVs in the HAT-P-12 system.

5. The Summary and Concluding Remark

This study investigates the Transit Timing Variations (TTVs) of the sub-Saturn mass planet HAT-P-12b around a metal-poor K4 dwarf star. By examining 46 transit light curves across a 14-year baseline, we analyze possible explanations for the variations in transit timings. We used four models to study TTVs: a linear, decay model, apsidal precession, and sinusoidal model. First, the transit timings were modeled using a linear model. This model assumes a constant orbital period and provides a baseline for detecting deviations. The $\chi^2_r = 8.1$ showed that the timing residuals exhibited non-random patterns. This finding strongly suggested that the orbit of HAT-P-12b has been affected by additional forces or interactions. We examined the possible effects of orbital decay, i.e. a steady decrease of the orbital period induced by tidal dissipation between the planet and its host star. The orbital decay model produced a lower $\chi^2_r = 6.3$, suggesting a better fit than the linear model. However, the computed stellar tidal quality ($Q_\star \sim 28.4$) was substantially below theoretical estimates $10^5 \leq Q_\star \leq 10^7$ for stars of similar properties. Therefore orbital decay is not the dominant mechanism in the HAT-P-12 system. The apsidal precession model, which incorporates a slight orbital eccentricity and a precession in the argument of periastron, provided the significantly lower $\chi^2_r = 4.2$ to the timing residuals than the linear and the decay model. The results show, a small eccentricity $e = 0.00130$ and the precession $\frac{dw}{dE} = 0.0045$ radians per epoch. To explore the possibility of a second planet in the system, we used the GLS periodogram to do a frequency analysis. Periodic signals that are not uniformly spaced in time-series data, such as transit times, can be found using this method. The GLS periodogram showed many prominent peaks, the most prominent of which corresponded to a frequency of $f_2 = 0.00415$ cycles per day. With a false alarm probability

(FAP) of 0.5×10^{-5} , this peak showed a highly significant periodic signal. To investigate further, we used a sinusoidal model to fit the timing residuals using the frequency values obtained from the GLS periodogram. The sinusoidal fit shows a lower $\chi^2_r = 3.2$ indicating the best model for the timing residuals. The amplitude of the best frequency $A_{TTV} = 2.6$ minutes. The periodic nature of the f2 signal strongly suggests the additional planetary companion in the HAT-P-12 system. Utilizing the amplitude and period of the sinusoidal signal, we estimated the mass of the perturbing planet to be approximately $0.02 M_J$, assuming a 2:1 Mean Motion Resonance (MMR). To verify that the timing residuals are not caused by stellar activity, we investigated the Applegate effect. However, this results in an amplitude of only 0.4 s, significantly less than the measured TTV amplitude of 156 seconds. Furthermore, the quasiperiodic changes usually associated with stellar activity contrast the truly periodic behavior of the observed signal. We therefore conclude that the observed TTVs are not likely to be caused by stellar activity. The perturbing planet's orbital period and estimated mass suggest a low-mass companion that could be located in a 2:1 mean-motion resonance with HAT-P-12b. We suggest that long-term observation and precise timing are required to discover the complex gravitational forces influencing planetary orbits. The work on HAT-P-12 could offer new perspectives on the dynamics of low-mass companions in sub-Saturn systems.

Acknowledgements

We are grateful to the anonymous referee for good suggestions. This project is supported in part by the National Science and Technology Council, Taiwan, under Ing-Guey Jiang's Grant NSTC 111-2112-M-007-035, NSTC 113-2112-M-007-030, and also Li-Chin Yeh's Grant NSTC 113-2115-M-007-008. P.T. expresses his sincere thanks to IUCAA, Pune, for providing support through the IUCAA Associateship Programme. V.K.M. acknowledge Govt. Niranjan Kesharwani College, Kota, Bilaspur (C.G.) for providing research facilities in the college.

References

A-thano, N., Jiang, I.G., Awiphan, S., Rattanamala, R., Su, L.H., Heng-piya, T., Sariya, D.P., Yeh, L.C., Shlyapnikov, A.A., Gorbachev, M.A., Rublevski, A.N., Mannaday, V.K., Thakur, P., Sahu, D.K., Mkrtichian, D.,

- Griv, E., 2022. The Transit Timing and Atmosphere of Hot Jupiter HAT-P-37b. *AJ* 163, 77. doi:10.3847/1538-3881/ac416d, arXiv:2112.04724.
- Agol, E., Steffen, J., Sari, R., Clarkson, W., 2005. On detecting terrestrial planets with timing of giant planet transits. *MNRAS* 359, 567–579. doi:10.1111/j.1365-2966.2005.08922.x.
- Alexoudi, X., Mallonn, M., von Essen, C., Turner, J.D., Keles, E., Southworth, J., Mancini, L., Ciceri, S., Granzer, T., Denker, C., Dineva, E., Strassmeier, K.G., 2018. Deciphering the atmosphere of HAT-P-12b: solving discrepant results. *A&A* 620, A142. doi:10.1051/0004-6361/201833691, arXiv:1810.02172.
- Applegate, J.H., 1992. A Mechanism for Orbital Period Modulation in Close Binaries. *ApJ* 385, 621. doi:10.1086/170967.
- Bakos, G., Noyes, R.W., Kovács, G., Stanek, K.Z., Sasselov, D.D., Domsa, I., 2004. Wide-Field Millimagnitude Photometry with the HAT: A Tool for Extrasolar Planet Detection. *PASP* 116, 266–277. doi:10.1086/382735, arXiv:astro-ph/0401219.
- Borucki, W.J., Koch, D.G., Basri, G., Batalha, N., Boss, A., Brown, T.M., Caldwell, D., Christensen-Dalsgaard, J., Cochran, W.D., DeVore, E., Dunham, E.W., Dupree, A.K., Gautier, III, T.N., Geary, J.C., Gilliland, R., Gould, A., Howell, S.B., Jenkins, J.M., Kjeldsen, H., Latham, D.W., Lissauer, J.J., Marcy, G.W., Monet, D.G., Sasselov, D., Tarter, J., Charbonneau, D., Doyle, L., Ford, E.B., Fortney, J., Holman, M.J., Seager, S., Steffen, J.H., Welsh, W.F., Allen, C., Bryson, S.T., Buchhave, L., Chandrasekaran, H., Christiansen, J.L., Ciardi, D., Clarke, B.D., Dotson, J.L., Endl, M., Fischer, D., Fressin, F., Haas, M., Horch, E., Howard, A., Isaacson, H., Kolodziejczak, J., Li, J., MacQueen, P., Meibom, S., Prsa, A., Quintana, E.V., Rowe, J., Sherry, W., Tenenbaum, P., Torres, G., Twicken, J.D., Van Cleve, J., Walkowicz, L., Wu, H., 2011. Characteristics of Kepler Planetary Candidates Based on the First Data Set. *ApJ* 728, 117. doi:10.1088/0004-637X/728/2/117, arXiv:1006.2799.
- Eastman, J., Gaudi, B.S., Agol, E., 2013. EXOFAST: A Fast Exoplanetary Fitting Suite in IDL. *PASP* 125, 83. doi:10.1086/669497, arXiv:1206.5798.

- Eastman, J., Siverd, R., Gaudi, B.S., 2010. Achieving Better Than 1 Minute Accuracy in the Heliocentric and Barycentric Julian Dates. *PASP* 122, 935. doi:10.1086/655938, arXiv:1005.4415.
- Espinoza, N., Kossakowski, D., Brahm, R., 2019. juliet: a versatile modelling tool for transiting and non-transiting exoplanetary systems. *MNRAS* 490, 2262–2283. doi:10.1093/mnras/stz2688, arXiv:1812.08549.
- Foreman-Mackey, D., Hogg, D.W., Lang, D., Goodman, J., 2013. emcee: The MCMC Hammer. *PASP* 125, 306. doi:10.1086/670067, arXiv:1202.3665.
- Giménez, A., Bastero, M., 1995. A Revision of the Ephemeris-Curve Equations for Eclipsing Binaries with Apsidal Motion. *Ap&SS* 226, 99–107. doi:10.1007/BF00626903.
- Hartman, J.D., Bakos, G.Á., Torres, G., Kovács, G., Noyes, R.W., Pál, A., Latham, D.W., Sipőcz, B., Fischer, D.A., Johnson, J.A., Marcy, G.W., Butler, R.P., Howard, A.W., Esquerdo, G.A., Sasselov, D.D., Kovács, G., Stefanik, R.P., Fernandez, J.M., Lázár, J., Papp, I., Sári, P., 2009. HAT-P-12b: A Low-Density Sub-Saturn Mass Planet Transiting a Metal-Poor K Dwarf. *ApJ* 706, 785–796. doi:10.1088/0004-637X/706/1/785, arXiv:0904.4704.
- Holman, M.J., Murray, N.W., 2005. The Use of Transit Timing to Detect Terrestrial-Mass Extrasolar Planets. *Science* 307, 1288–1291. doi:10.1126/science.1107822, arXiv:astro-ph/0412028.
- Jiang, I.G., Lai, C.Y., Savushkin, A., Mkrtichian, D., Antonyuk, K., Griv, E., Hsieh, H.F., Yeh, L.C., 2016. The Possible Orbital Decay and Transit Timing Variations of the Planet WASP-43b. *AJ* 151, 17. doi:10.3847/0004-6256/151/1/17, arXiv:1511.00768.
- Jiang, I.G., Yeh, L.C., Thakur, P., Wu, Y.T., Chien, P., Lin, Y.L., Chen, H.Y., Hu, J.H., Sun, Z., Ji, J., 2013. Possible Transit Timing Variations of the TrES-3 Planetary System. *AJ* 145, 68. doi:10.1088/0004-6256/145/3/68, arXiv:1308.2456.
- Kokori, A., Tsiaras, A., Edwards, B., Rocchetto, M., Tinetti, G., Wiünsche, A., Paschalis, N., Agnihotri, V.K., Bachschmidt, M., Bretton, M., Caines,

- H., Caló, M., Casali, R., Crow, M., Dawes, S., Deldem, M., Deligeorgopoulos, D., Dymock, R., Evans, P., Falco, C., Ferratflat, S., Fowler, M., Futcher, S., Guerra, P., Hurter, F., Jones, A., Kang, W., Kim, T., Lee, R., Lopresti, C., Marino, A., Mallonn, M., Mortari, F., Morvan, M., Mugnai, L.V., Nastasi, A., Perroud, V., Pereira, C., Phillips, M., Pintr, P., Raetz, M., Regembal, F., Savage, J., Sedita, D., Sioulas, N., Strikis, I., Thurston, G., Tomacelli, A., Tomatis, A., 2022. ExoClock project: an open platform for monitoring the ephemerides of Ariel targets with contributions from the public. *Experimental Astronomy* 53, 547–588. doi:10.1007/s10686-020-09696-3, arXiv:2012.07478.
- Lee, J.W., Youn, J.H., Kim, S.L., Lee, C.U., Hinse, T.C., 2012. The Sub-Saturn Mass Transiting Planet HAT-P-12b. *AJ* 143, 95. doi:10.1088/0004-6256/143/4/95, arXiv:1201.6419.
- Lithwick, Y., Xie, J., Wu, Y., 2012. Extracting Planet Mass and Eccentricity from TTV Data. *ApJ* 761, 122. doi:10.1088/0004-637X/761/2/122, arXiv:1207.4192.
- Lomb, N.R., 1976. Least-Squares Frequency Analysis of Unequally Spaced Data. *Ap&SS* 39, 447–462. doi:10.1007/BF00648343.
- Maciejewski, G., Dimitrov, D., Fernández, M., Sota, A., Nowak, G., Ohlert, J., Nikolov, G., Bukowiecki, Ł., Hinse, T.C., Pallé, E., Tingley, B., Kjurkchieva, D., Lee, J.W., Lee, C.U., 2016. Departure from the constant-period ephemeris for the transiting exoplanet WASP-12. *A&A* 588, L6. doi:10.1051/0004-6361/201628312, arXiv:1602.09055.
- Maciejewski, G., Dimitrov, D., Neuhäuser, R., Niedzielski, A., Raetz, S., Ginski, C., Adam, C., Marka, C., Moualla, M., Mugrauer, M., 2010. Transit timing variation in exoplanet WASP-3b. *MNRAS* 407, 2625–2631. doi:10.1111/j.1365-2966.2010.17099.x, arXiv:1006.1348.
- Maciejewski, G., Fernández, M., Aceituno, F., Martín-Ruiz, S., Ohlert, J., Dimitrov, D., Szyszka, K., von Essen, C., Mugrauer, M., Bischoff, R., Michel, K.U., Mallonn, M., Stangret, M., Moździerski, D., 2018. Planet-Star Interactions with Precise Transit Timing. I. The Refined Orbital Decay Rate for WASP-12 b and Initial Constraints for HAT-P-23 b, KELT-1 b, KELT-16 b, WASP-33 b and WASP-103 b. *Acta Astron.* 68, 371–401. doi:10.32023/0001-5237/68.4.4, arXiv:1812.02438.

Maciejewski, G., Sierzputowska, J., Golonka, J., 2023. Search for Planets in Hot Jupiter Systems with Multi-Sector TESS Photometry. IV. Null Detections in 12 Systems. *Acta Astron.* 73, 159–177. doi:10.32023/0001-5237/73.2.3, arXiv:2312.03319.

Mallonn, M., Nascimbeni, V., Weingrill, J., von Essen, C., Strassmeier, K.G., Piotto, G., Pagano, I., Scandariato, G., Csizmadia, S., Herrero, E., Sada, P.V., Dhillon, V.S., Marsh, T.R., Künstler, A., Bernt, I., Granzer, T., 2015. Broad-band spectrophotometry of the hot Jupiter HAT-P-12b from the near-UV to the near-IR. *A&A* 583, A138. doi:10.1051/0004-6361/201425395, arXiv:1509.05272.

Mancini, L., Esposito, M., Covino, E., Southworth, J., Biazzo, K., Bruni, I., Ciceri, S., Evans, D., Lanza, A.F., Poretti, E., Sarkis, P., Smith, A.M.S., Brogi, M., Affer, L., Benatti, S., Bignamini, A., Boccato, C., Bonomo, A.S., Borsa, F., Carleo, I., Claudi, R., Cosentino, R., Damasso, M., Desidera, S., Giacobbe, P., González-Álvarez, E., Gratton, R., Harutyunyan, A., Leto, G., Maggio, A., Malavolta, L., Maldonado, J., Martinez-Fiorenzano, A., Masiero, S., Micela, G., Molinari, E., Nascimbeni, V., Pagano, I., Pedani, M., Piotto, G., Rainer, M., Scandariato, G., Smareglia, R., Sozzetti, A., Andreuzzi, G., Henning, T., 2018. The GAPS programme with HARPS-N at TNG. XVI. Measurement of the Rossiter-McLaughlin effect of transiting planetary systems HAT-P-3, HAT-P-12, HAT-P-22, WASP-39, and WASP-60. *A&A* 613, A41. doi:10.1051/0004-6361/201732234, arXiv:1802.03859.

Mandel, K., Agol, E., 2002. Analytic Light Curves for Planetary Transit Searches. *ApJ* 580, L171–L175. doi:10.1086/345520, arXiv:astro-ph/0210099.

Mannaday, V.K., Thakur, P., Jiang, I.G., Sahu, D.K., Joshi, Y.C., Pandey, A.K., Joshi, S., Yadav, R.K., Su, L.H., Sariya, D.P., Yeh, L.C., Griv, E., Mkrtichian, D., Shlyapnikov, A., Moskvin, V., Ignatov, V., Vaňko, M., Püsküllü, Ç., 2020. Probing Transit Timing Variation and Its Possible Origin with 12 New Transits of TrES-3b. *AJ* 160, 47. doi:10.3847/1538-3881/ab9818, arXiv:2006.00599.

Mannaday, V.K., Thakur, P., Southworth, J., Jiang, I.G., Sahu, D.K., Mancini, L., Vaňko, M., Kundra, E., Gajdoš, P., A-thano, N., Sariya, D.P.,

- Yeh, L.C., Griv, E., Mkrtichian, D., Shlyapnikov, A., 2022. Revisiting the Transit Timing Variations in the TrES-3 and Qatar-1 Systems with TESS Data. *AJ* 164, 198. doi:10.3847/1538-3881/ac91c2, arXiv:2209.04080.
- McCullough, P.R., Stys, J.E., Valenti, J.A., Fleming, S.W., Janes, K.A., Heasley, J.N., 2005. The XO Project: Searching for Transiting Extrasolar Planet Candidates. *PASP* 117, 783–795. doi:10.1086/432024, arXiv:astro-ph/0505560.
- Öztürk, O., Erdem, A., 2019. New photometric analysis of five exoplanets: CoRoT-2b, HAT-P-12b, TrES-2b, WASP-12b, and WASP-52b. *MNRAS* 486, 2290–2307. doi:10.1093/mnras/stz747.
- Patra, K.C., Winn, J.N., Holman, M.J., Yu, L., Deming, D., Dai, F., 2017. The Apparently Decaying Orbit of WASP-12b. *AJ* 154, 4. doi:10.3847/1538-3881/aa6d75, arXiv:1703.06582.
- Penev, K., Bouma, L.G., Winn, J.N., Hartman, J.D., 2018. Empirical Tidal Dissipation in Exoplanet Hosts From Tidal Spin-up. *AJ* 155, 165. doi:10.3847/1538-3881/aaaf71, arXiv:1802.05269.
- Pollacco, D.L., Skillen, I., Collier Cameron, A., Christian, D.J., Hellier, C., Irwin, J., Lister, T.A., Street, R.A., West, R.G., Anderson, D.R., Clarkson, W.I., Deeg, H., Enoch, B., Evans, A., Fitzsimmons, A., Haswell, C.A., Hodgkin, S., Horne, K., Kane, S.R., Keenan, F.P., Maxted, P.F.L., Norton, A.J., Osborne, J., Parley, N.R., Ryans, R.S.I., Smalley, B., Wheatley, P.J., Wilson, D.M., 2006. The WASP Project and the SuperWASP Cameras. *PASP* 118, 1407–1418. doi:10.1086/508556, arXiv:astro-ph/0608454.
- Sariya, D.P., Jiang, I.G., Su, L.H., Yeh, L.C., Chang, T.E., Moskvin, V.V., Shlyapnikov, A.A., Ignatov, V., Mkrtichian, D., Griv, E., Mannaday, V.K., Thakur, P., Sahu, D.K., Chand, S., Bisht, D., Sun, Z., Ji, J., 2021. Non-sinusoidal transit timing variations for the exoplanet HAT-P-12b. *Research in Astronomy and Astrophysics* 21, 097. doi:10.1088/1674-4527/21/4/97, arXiv:2012.08820.
- Scargle, J.D., 1982. Studies in astronomical time series analysis. II. Statistical aspects of spectral analysis of unevenly spaced data. *ApJ* 263, 835–853. doi:10.1086/160554.

- Seager, S., Deming, D., 2010. Exoplanet Atmospheres. *ARA&A* 48, 631–672. doi:10.1146/annurev-astro-081309-130837, arXiv:1005.4037.
- Southworth, J., Dominik, M., Jørgensen, U.G., Andersen, M.I., Bozza, V., Burgdorf, M.J., D’Ago, G., Dib, S., Figuera Jaimes, R., Fujii, Y.I., Gill, S., Haikala, L.K., Hinse, T.C., Hundertmark, M., Khalouei, E., Korhonen, H., Longa-Peña, P., Mancini, L., Peixinho, N., Rabus, M., Rahvar, S., Sajadian, S., Skottfelt, J., Snodgrass, C., Spyros, P., Tregloan-Reed, J., Unda-Sanzana, E., von Essen, C., 2019. Transit timing variations in the WASP-4 planetary system. *MNRAS* 490, 4230–4236. doi:10.1093/mnras/stz2602, arXiv:1907.08269.
- Todorov, K.O., Deming, D., Knutson, H.A., Burrows, A., Fortney, J.J., Lewis, N.K., Cowan, N.B., Agol, E., Desert, J.M., Sada, P.V., Charbonneau, D., Laughlin, G., Langton, J., Showman, A.P., 2013. Warm Spitzer Photometry of Three Hot Jupiters: HAT-P-3b, HAT-P-4b and HAT-P-12b. *ApJ* 770, 102. doi:10.1088/0004-637X/770/2/102, arXiv:1305.0833.
- von Essen, C., Wedemeyer, S., Sosa, M.S., Hjorth, M., Parkash, V., Freudenthal, J., Mallonn, M., Miculán, R.G., Zibecchi, L., Cellone, S., Torres, A.F., 2019. Indications for transit-timing variations in the exo-Neptune HAT-P-26b. *A&A* 628, A116. doi:10.1051/0004-6361/201731966, arXiv:1904.06360.
- Watson, C.A., Marsh, T.R., 2010. Orbital period variations of hot Jupiters caused by the Applegate effect. *MNRAS* 405, 2037–2043. doi:10.1111/j.1365-2966.2010.16602.x, arXiv:1003.0340.
- Wolf, A.S., Ragozzine, D., 2009. Probing the Interiors of Very Hot Jupiters Using Transit Light Curves, in: Pont, F., Sasselov, D., Holman, M.J. (Eds.), *Transiting Planets*, pp. 163–169. doi:10.1017/S1743921308026367.
- Yee, S.W., Winn, J.N., Knutson, H.A., Patra, K.C., Vissapragada, S., Zhang, M.M., Holman, M.J., Shporer, A., Wright, J.T., 2020. The Orbit of WASP-12b is Decaying, in: American Astronomical Society Meeting Abstracts #235, p. 456.02.

Yeh, L.C., Jiang, I.G., A-thano, N., 2024. Searching for candidates of orbital decays among transit exoplanets. *New Astronomy* 106, 102130. doi:10.1016/j.newast.2023.102130, arXiv:2310.08953.

Zechmeister, M., Kürster, M., 2009. The generalised Lomb-Scargle periodogram. A new formalism for the floating-mean and Keplerian periodograms. *A&A* 496, 577–584. doi:10.1051/0004-6361:200811296, arXiv:0901.2573.